Assessment of physical/mechanical properties and cytotoxicity of dual-cured resin cements containing Sr-bioactive glass nanoparticles and calcium phosphate

Sasipin THANYASIRI[1], Parichart NARUPHONTJIRAKUL[2], Chawal PADUNGLAPPISIT[1], Bharat MIRCHANDANI[3], Anne M. YOUNG[4] and Piyaphong PANPISUT[1,5]

[1] *Faculty of Dentistry, Thammasat University, Pathum Thani 12120, Thailand*
[2] *Biological Engineering Program, Faculty of Engineering, King Mongkut's University of Technology Thonburi, Bangkok 10140, Thailand*
[3] *Faculty of Dentistry, Datta Meghe Institute of Higher Education & Research, Sawangi (Meghe), Wardha, Maharashtra 442001, India*
[4] *Division of Biomaterials and Tissue Engineering, UCL Eastman Dental Institute, Royal Free Hospital, Rowland Hill Street, London, NW3 2PF, UK*
[5] *Thammasat University Research Unit in Dental and Bone Substitute Biomaterials, Thammasat University, Pathum Thani 12120, Thailand*
Corresponding author, Piyaphong PANPISUT; E-mail: panpisut@tu.ac.th

The aim was to develop dual-cured resin cements containing Sr-bioactive glass nanoparticles (Sr-BGNPs; 5 or 10 wt%) and monocalcium phosphate monohydrate (MCPM; 3 or 6 wt%). Effects of additives on degree of monomer conversion (DC), biaxial flexural strength/modulus, shear bond strength (SBS), mass/volume change, color stability, ion release, and cytotoxicity were examined. Controls included material without reactive fillers and Panavia SA Plus (PV). Experimental cements showed higher DC than PV regardless of light activation ($p<0.05$). Mean SBS and color stability were comparable between experimental cements and PV. Cell viability upon the exposure to sample extracts of experimental cements was 80%–92%. High additive concentrations led to lower strength and modulus than PV ($p<0.05$). The additives increased mass change, reduced color stability, and promoted ion release. The experimental resin cements demonstrated acceptable mechanical/chemical properties and cytotoxicity. The additives reduced the strength but provided ion release, a desirable action to prevent recurrent caries.

Keywords: Resin cements, Bioactive glass, Calcium phosphate, Polymerization, Flexural strength

INTRODUCTION

Indirect restorations or fixed dental prostheses are needed for restoring severely damaged permanent teeth[1]. These treatments require cementation steps to fix the restoration to the tooth structure. It was reported that secondary caries is one of the major causes of failure for indirect restorations[2-5]. A possible cause could be due to the inadequate marginal seal at the cement interface may result in an irregular surface or microleakage[6]. This may promote the accumulation of food debris, dental biofilms[7,8], marginal discoloration[6], and tooth demineralization. Such failure could potentially lead to pulpal complications, requiring complicated restorative treatments or tooth extraction[9].

Resin cements capable of ion release may promote remineralization to control dental caries at the tooth-restoration interace[10,11]. The mineralizing actions of these cements may shift the caries balance toward mineral gain, thus controlling caries[12,13]. The release of calcium and phosphate ions is essential for encouraging the mineralizing actions for resin composites or dental adhesives. This can be achieved by the incorporating of monocalcium phosphate monohydrate (MCPM) or tricalcium phosphate[14-18]. A primary concern with hydrophilic calcium phosphate fillers is the increase in water sorption, which can reduce the physical and mechanical properties of resin-based materials over time[19]. The absorption of water, which act as plasticizer, may reduce polymer rigidity, strength, and color/optical properties of dental materials[20]. This may subsequently compromise the functions of restorations. However, water sorption is essential for solubilizing calcium phosphate and enabling ion release[21].

The incorporation of antimicrobial agents was expected to decrease bacterial colonization[22]. The use of bioactive glass nanoparticles enabled both remineralization and antibacterial actions[23]. The release of multiple ions, such as Ca, Si, P, and Sr, may contribute to the enhanced antibacterial actions. These ions could potentially modify osmotic pressure or pH, thereby promoting an environment that could reduce bacterial colonization[24-26]. Moreover, the release of Sr ion inhibited the growth and reproduction, synthesis of cell walls, cell metabolism, and chromosomal replication of bacteria[25]. Furthermore, a study reported that Sr enhanced weak antibacterial action but also promoted radiopacity and dentin remineralization[27]. It was reported that the biological and chemical effects of bioactive glass on cells were influenced by particle diameter[28]. Hence, their potential cytotoxic effect is of concern.

This study's objective was to prepare resin cements that exhibit ion-releasing action. Additionally, the effects of incorporating varying concentrations of Sr-bioactive glass nanoparticles (Sr-BGNPs; 5 or 10 wt%) and MCPM (3 or 6 wt%) were determined. Effects of the fillers on the degree of monomer conversion, biaxial flexural strength and modulus, shear bond strength with ceramic, color stability, mass/volume changes, ion release, and cytotoxicity of restorative materials. This study's

hypotheses were as follows: (i) different concentrations of Sr-BGNPs and MCPM show no significant effects on the tested properties of resin cements, and (ii) the physical/mechanical properties of experimental resin cements shall not differ significantly from those of a commercial resin cement.

MATERIALS AND METHODS

Synthesis of Sr-BGNPs

Sr-BGNPs were synthesized using a protocol described in a previous study[18] and all chemicals in the protocol were purchased from Sigma-Aldrich (St. Louis, MO, USA). Silica nanoparticles were first synthesized, followed by ion incorporation through a post-functionalization process. A base catalyst (ammonium hydroxide) was employed to control particle's size and decrease particle agglomeration[29]. A purified water (12.3 mL) was mixed with ammonium hydroxide (1.5 mL), and ethyl alcohol (98.7 mL) and stirred (600 rpm) in a 250 mL Erlenmeyer flask for 30 min. Then, the mixture was added with 7.5 mL of tetraethyl orthosilicate and stirred for an additional 8 h to complete the reaction. The obtained suspension was centrifuged to collect the silica nanoparticles. The obtained particles were resuspended in deionized water and then doped with calcium (Ca) and strontium (Sr) through the addition of calcium nitrate tetrahydrate (3.97 g) and strontium nitrate (10.67 g). The nominal molar ratio of Si:Ca:Sr was 1:0.5:1.5. The obtained particles were dried and heated (heating rate of 3°C/min) until the temperature reached 680°C. A heat treatment process at 680°C (holding time of 3 h) was used to dope the glass particles with Ca and Sr.

After washing with ethanol, the particles were coated for 45 s with gold at a current of 23 mA (Q150R ES, Quorum Technologies, East Sussex, UK). Particle size and composition were then examined using a scanning electron microscope (SEM; JSM 7800F, JEOL, Tokyo, Japan) with an energy-dispersive X-ray instrument (EDX; X-Max 20, Oxford Instruments, Abingdon, UK).

Preparation of experimental resin cements

The liquid phase of the experimental resin cements was prepared as in previous studies (Table 1)[20,30]. It contained urethane dimethacrylate (UDMA; Sigma-Aldrich), triethyleneglycol dimethacrylate (TEGDMA; Sigma-Aldrich), 2-hydroxyethyl methacrylate (HEMA; Sigma-Aldrich), 10-methacryloyloxydecyl dihydrogen phosphate (10-MDP; Watson International, Jiangsu, China), and camphorquinone (CQ; Sigma-Aldrich). Additionally, benzoyl peroxide (BPO; Sigma-Aldrich) and N-dimethyl-p-toluidine (DMPT; Sigma-Aldrich) were used as an initiator and activator, respectively.

The powder phase of the cement contained silanated boroaluminosilicate glass (Esstech, Essington, PA, USA), Sr-BGNPs, and MCPM (Himed, Old Bethpage, NY, USA). Powders were formulated with varying levels of Sr-BGNPs (10 or 5 wt%) and MCPM (6 or 3 wt%), and a control was prepared without either of these materials (Fig. 1, Table 2). Each formulation's powder phase was manually mixed with initiator or activator liquids at
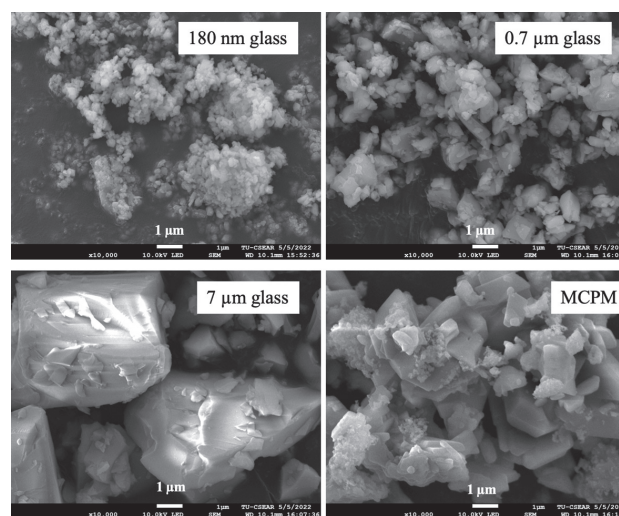

Fig. 1   SEM image of powder phase.

Table 1   Composition (wt%) of the liquid phases

Liquid formulation	UDMA	TEGDMA	HEMA	10-MDP	BP	CQ	DMPT
Initiator liquid	70	22.75	3	3	0.75	0.5	0
Activator liquid	70	22.75	3	3	0	0.5	0.75

Table 2   Composition (wt%) of the experimental resin cements

Formulation/component (approximate particle diameter)	M6S10	M6S5	M3S10	M3S5	M0S0
Boroaluminosilicate glass (7 μm)	33.6	35.6	34.8	36.8	40
Boroaluminosilicate glass (0.7 μm)	33.6	35.6	34.8	36.8	40
Boroaluminosilicate glass (180 nm)	16.8	17.8	17.4	18.4	20
MCPM (10 μm)	6	6	3	3	0
Sr-BGNPs (200 nm)	10	5	10	5	0

Table 3　Composition of the commercial comparison (Panavia SA Cement Plus)

Material	Component	Instruction
Panavia SA Cement Plus (PV)	bisphenol-A-diglycidyl methacrylate, triethylene glycol dimethacrylate, 2-hydroxyethyl methacrylate, sodium fluoride, silanated barium glass filler, silanated colloidal silica, 10-methacryloyloxydecyl dihydrogen phosphate, hydrophobic aromatic dimethacrylate, hydrophobic aliphatic dimethacrylate, dl-camphorquinone, peroxide, accelerators, catalysts, pigments	Attach mixing tip and extrude the two pastes. Light cure for 10 s.

a ratio of 2.7:1 (mass ratio) for 20 s until homogenous appearances were obtained. The mixed pastes were loaded into double-barrel syringes (medmix Switzerland, Haag, Switzerland). The cements were mixed using the syringe mixing tip and dispenser (medmix Switzerland). The commercial self-adhesive resin cement for comparison was Panavia SA cement plus (lot no. 210308, Kuraray Noritake Dental, Okayama, Japan) (Table 3).

Degree of monomer conversion (DC)
The DC of materials was determined using an attenuated total reflectance-Fourier transform infrared spectroscopy (ATR-FTIR; Nicolet iS5, Thermo Fisher Scientific, Waltham, MA, USA) (*n*=6). For DC upon light activation, the cements were injected into a metal ring (10 mm in diameter and 1 mm in thickness) placed over the ATR diamond. The FTIR spectra (700–4,000 cm^{-1}) with 8 repetitions and a resolution of 4 cm^{-1} were obtained from the bottom of the specimen at initially and after curing for 20 s. The specimens were cured with an LED light-curing unit (irradiance of 1,200 mW/cm^2, SmartLite Focus Pen Style, DENTSPLY Sirona, York, PA, USA). The distance between the light-curing and specimen's surface was approximately 1 mm. The equation for calculating DC is provided as follow[20].

$$DC = \frac{100\,(\Delta A_o - \Delta A_t)}{\Delta A_o} \qquad \text{Equation 1}$$

where ΔA_o and ΔA_t represent the peak's height at of C-O of methacrylate group (1,320 cm^{-1})[31] above the background level at 1,335 cm^{-1} before curing and at the time (t) after initiating curing, respectively. For conversion without light activation, the cements were placed on the ATR diamond and covered with a metal plate to avoid any exposure to natural light. Then, FTIR spectra were recorded from the bottom of specimens for 30 min. The linear extrapolation of late-time DC was then calculated[30].

Biaxial flexural strength (BFS) and modulus of elasticity (BFM)
The BFS and BFM of the materials were assessed using a ball-on-ring testing jig and a mechanical testing frame (AGSX, Shimadzu, Kyoto, Japan) (*n*=7)[15]. Disc specimens (10 mm in diameter and 1 mm in thickness) were produced using a metal ring (Springmasters, Redditch, UK). The specimens were covered on top and bottom surfaces with acetate sheets. They were light-

cured for 20 s on each side with an LED light-curing unit[32]. The specimens were allowed to post-cure at room temperature for an additional 24 h[33]. Then, the specimens were removed from the ring and placed in deionized water (10 mL) for 24 h and 4 weeks at 37°C. The thickness of each specimen was measured with a vernier caliper. They were subjected to a 500 N load cell and 1 mm/min crosshead speed. The BFS (Pa) and BFM (Pa) were analyzed using the following equations.

$$BFS = \frac{F}{d^2}\{(1+v)[0.485\ln(\frac{r}{d})+0.52]+0.48\} \quad \text{Equation 2}$$

$$BFM = (\frac{\Delta H}{\Delta W_c}) \times (\frac{\beta_c d^2}{q^3}) \qquad \text{Equation 3}$$

Where F is the failure load (N), d represents the thickness of the disc specimens (m), r represents the radius of the circular support of the ball-on-ring testing jig (m), and v represents Poisson's ratio (0.3)[34]. Furthermore, $\frac{\Delta H}{\Delta W_c}$ represents the rate of change of the load about the central deflection or gradient of force versus the displacement curve (N/m)[18]. β_c and q represent the center deflection function (0.5024) and the ratio of the support radius to the specimen radius, respectively. The fracture surfaces of representative specimens of each material were additionally examined using SEM-EDX.

Shear bond strength (SBS) to lithium disilicate ceramic (LDS)
The macro-SBS of resin cements to LDS was tested using a SBS testing jig (*n*=6)[35]. LDS plates (dimensions of 14.5×14.5×1.5 mm^3, IPS E.max CAD, Ivoclar Vivadent, Schaan, Liechtenstein) were cut (Accutom-50, Struers, Cleveland, OH, USA), followed the sintering in a high-temperature furnace (Ivoclar EP3000, Volar Vivadent). The heating rate was 60°C/min with a holding time of 15 min at the final temperature of 815°C. The plates were embedded in an autopolymerizing acrylic resin. Bonding surfaces were then polished using 220, 320, 500, and 800-grit silicon carbide abrasive papers under water coolant using a polishing machine (Tegramin-25, Struers). They were subsequently washed in an ultrasonic bath for 10 min. The exposed bonding surface of the LDS was etched with 4.5% hydrofluoric acid for

20 s and then thoroughly washed with water and air-dried. Then, the surface was cleaned using a universal cleaning paste (Ivoclean, Ivoclar Vivadent) for 20 s. The surface was again washed for 20 s with a water syringe and air-dried for 10 s. Prior to the addition of cements, a primer (Clearfil ceramic primer plus, Kuraray Noritake Dental) was applied to the LDS surface, which was then air-dried for 10 s.

The cements were injected into a mold (Ultradent Products, South Jordan, UT, USA) on the LDS surface to produce a cylinder (2.38 mm in diameter and 3 mm in height). The excess cement was removed with a microbrush and cured using an LED light-curing unit for 40 s. The jig was then removed. The specimens were left at room temperature for 24 h. They were then placed in deionized water and maintained at 37°C for 24 h. The SBS was tested using a SBS testing jig and a universal testing machine. The test was conducted using a 500 N load cell and a crosshead speed of 1 mm/min. The SBS (Pa) was then calculated (Equation 4).

$$SBS = \frac{F}{A} \qquad \text{Equation 4}$$

Where F and A represent the load at failure (N) and the area of the bonding interface (m^2), respectively. The failure mode at the ceramic-cement interface was examined with a stereomicroscope (Leica Zoom 2000, Leica Microsystems, Wetzlar, Germany).

Color changes or color stability (ΔE^*_{00})
An intraoral digital spectrophotometer (Easyshade V, VITA Zahnfabrik, Bad Säckingen, Germany) was employed to assess the color stability (ΔE^*_{00}) of the materials after immersion in deionized water. The test was conducted following a protocol described in a previous study[20]. Disc specimens (1 mm thick and 10 mm in diameter) were prepared as described above (n=5). They were immersed in deionized water (10 mL) and kept at 37°C. The measurement of CIELAB coordinates (CIE L^*, a^*, b^*, C^*, and h^o) for the samples were performed before water immersion and at 24 h and 4 weeks of water storage. Lightness and values on the red-green and yellow-blue axes are indicated by L^*, a^*, and b^*. The chroma and hue angle are represented by C^* and h^o, respectively. The CIEDE2000 formula (equation 5)[36] was used o determine the changes in color or color stability (ΔE^*_{00}) upon immersion in water.

$$\Delta E^*_{00} = [(\frac{\Delta L'}{K_L S_L}) + (\frac{\Delta C'}{K_C S_C}) + (\frac{\Delta H'}{K_H S_H}) + R_T (\frac{\Delta C'}{K_C S_C})(\frac{\Delta H'}{K_H S_H})]^{1/2}$$
$$\text{Equation 5}$$

where $\Delta L'$, $\Delta C'$, and $\Delta H'$ represent the differences in lightness, chroma, and hue, respectively, before and after immersion. R_T is a rotation function related to the interaction between the chroma and hue differences in the blue region. Furthermore, S_L, S_C, and S_H are weighting functions, and K_L, K_C, K_H are the correction terms for experimental conditions. The complete formulae were provided in a previous study[36].

Mass and volume changes in water
Gravimetric studies were employed to determine the mass/volume changes of the materials (n=5). Disc specimens (1 mm in thickness and 10 mm in diameter) were prepared and placed in deionized water (10 mL) at 37°C. The mass and volume of the specimens were recorded for up to 8 weeks using an analytical scale and density kit (MS-DNY-43, METTLER TOLEDO, Columbus, OH, USA)[37]. The changes of mass and volume of specimens upon water immersion were calculated using the following equations.

$$\Delta M = \frac{100[M_t - M_o]}{M_o} \qquad \text{Equation 6}$$

$$\Delta V = \frac{100[V_t - V_o]}{V_o} \qquad \text{Equation 7}$$

where M_t and V_t represent the mass and volume of the specimens obtained at time t, respectively. Additionally, M_o and V_o represent the mass and volume of the specimens recorded initially before immersion, respectively.

Ion release
The inductively coupled plasma–atomic emission spectroscopy (ICP-OES, Optima 8300, PerkinElmer, Waltham, MA, USA) was employed to measure the release of Ca, Sr, and P ions in deionized water. Disc specimens (1 mm thick and 10 mm in diameter) were placed in deionized water (10 mL) and kept at 37°C (n=5). The water was collected and refreshed with a new solution at 24 h, 2 weeks, and 4 weeks. Prior to analysis, the storage solutions were mixed with 3 vol% nitric acid. Instrument calibration was conducted using a calibration standard (PerkinElmer Plus, PerkinElmer). The detection thresholds for Ca, Sr, and P were 0.1–50 ppm, 0.1–50 ppm, and 0.5–20 ppm, respectively. The results were displayed as cumulative release values.

Cytotoxicity
Cytotoxicity testing of the extracts from disc specimens was performed using a protocol described in a previous study[38]. Disc specimens (0.5 mm thick and 6 mm in diameter) were prepared and sterilized under UV irradiation for 30 min on both top and bottom sides (n=3). The specimens were placed in 200 μL of Dulbecco's modified Eagle medium (DMEM; Gibco, Thermo Fisher Scientific, Grand Island, NY, USA) added with 10% FBS (Gibco, Thermo Fisher Scientific), 1% penicillin/streptomycin (Gibco, Thermo Fisher Scientific) and 1% L-glutamine (Gibco, Thermo Fisher Scientific). The specimens were left for 5 h at room temperature, the specimens were removed. Then, the medium was pipetted (50 μL, mixed with an equal volume of fresh medium (two-fold dilution), and subsequently placed into 96-well plates. The plates were then seeded with mouse fibroblast L292 cells (density of 8×10^3 cells/well).

The negative control was plain culture medium.

The cells were cultured at 37°C in a humidified atmosphere containing 5% CO_2 for 72 h. Subsequently, the MTT solution (0.5 mg/mL, Invitrogen, Thermo Fisher Scientific) was added to each well for 30 min. The reaction was terminated by 100 μL of dimethylsulfoxide (Sigma-Aldrich) The final product's color, with the absorbance measured at 570 and 650 nm (OD, optical density), was recorded using a microplate reader spectrophotometer (Varioskan LUX Multimode, Thermo Fisher Scientific). The results were present as the relative cell viability (%) compared with the control using the following equation[39,40]. The test was conducted in triplicate.

$$\text{Relative cell viability} = \frac{\text{OD of the test group}}{\text{OD of the control}} \times 100$$

Equation 8

Statistical analysis
The values reported in the current study are means and SDs. Statistical analysis was performed using GraphPad Prism 9.4.0 for Mac OS (GraphPad Software, San Diego, CA, USA). The data were first determined for normality by Shapiro-Wilk test. Then the data were analyzed by one-way ANOVA followed by *post hoc* pairwise comparisons using Tukey's HSD. Paired *t*-tests and one-way repeated ANOVA were additionally employed to analyze the color stability and ion release of the materials at different time points. The significance

value was set at $p=0.05$.

G*Power version 3.1.9.6 (University of Düsseldorf, Düsseldorf, Germany) was employed to perform power analysis using results from previous studies to calculate the effect size (Cohen's f) and the sample size. The protocols were provided in previously published studies[41,42]. The sample size was chosen to provide a power greater than 0.95 at alpha=0.05 using one-way ANOVA. In addition, a factorial analysis was used to analyze the effect of increasing concentrations of MCPM (from 3 to 6 wt%) and Sr-BGNPs (from 5 to 10 wt%) on the tested properties[15].

RESULTS

Preparation of Sr-BGNPs
The SEM images indicated that spherical, monodisperse Sr-BGNPs had a diameter of approximately 100 nm (Fig. 2A). Ca and Sr were detected on the surface of the particles (Fig. 2B). These ions, however, exhibited a minimal effect on the FTIR spectrum (Fig. 2C). There was a broad band from 1,200 to 1,000 cm^{-1} due to an asymmetric Si–O–Si stretching vibration. The peak at approximately 800 cm^{-1} and 460 cm^{-1} were consistent with a symmetric Si-O stretching vibration and Si-O-Si rocking, respectively[43]. Furthermore, the XRD pattern of the particles revealed broad diffraction halos at approximately 20–30 (2Θ), which represent an amorphous state (Fig. 2D).

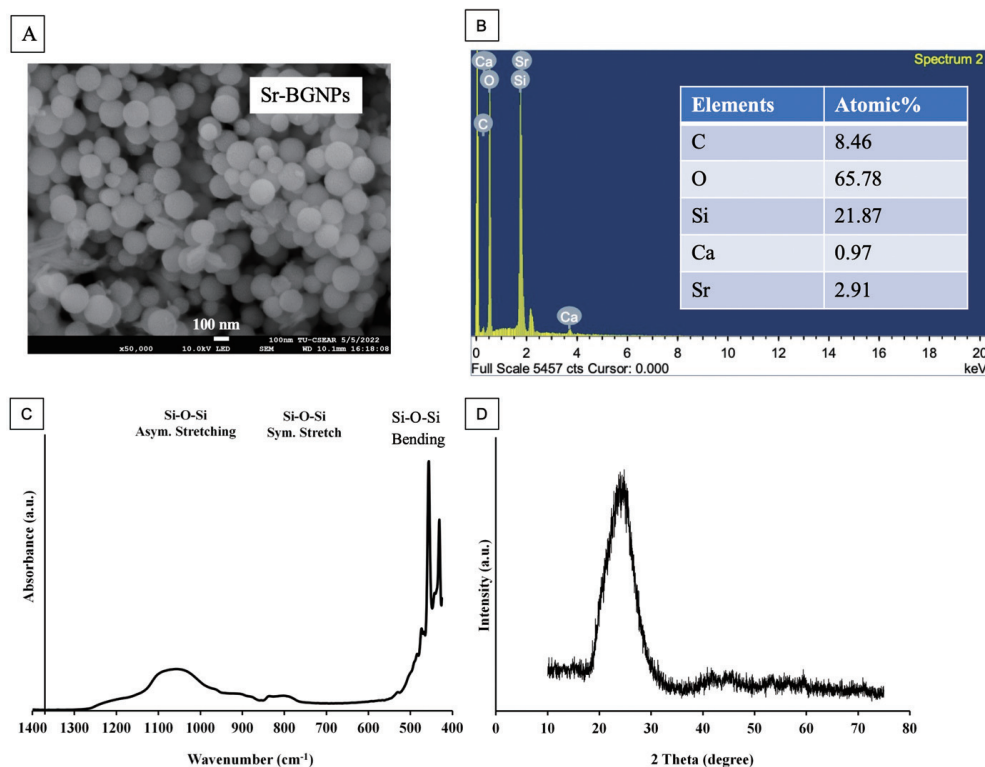| Elements	Atomic%
C	8.46
O	65.78
Si	21.87
Ca	0.97
Sr	2.91

Fig. 2 (A) SEM image demonstrating spherical particles of Sr-BGNPs, and (B) the elemental composition, (C) FTIR spectrum, and (D) XRD pattern of Sr-BGNPs.

DC

The highest and lowest DCs with light activation were measured for M0S0 (63.5±2.0) and PV (33.6±3.2), respectively (Fig. 3A). That of PV was significantly lower than that of M6S10 (61.2±1.4%), M6S5 (58.7±6.3%, $p<0.001$), M3S10 (62.4±2.0%, $p<0.001$), M3S5 (62.2±1.4%, $p<0.001$), and M0S0 ($p<0.001$). The DC without light activation of PV (46.1±3.3) was also lower than that of all experimental resin cements. Additionally, the DC without light activation of experimental resin cements increased more rapidly than that of PV (Fig. 3B). A significant difference in DC with and without light activation was detected for M6S5 ($p=0.0002$) and PV ($p<0.001$). Furthermore, factorial analysis indicated that increasing Sr-BGNPs and MCPM concentrations had a negligible effect on the final DC.

BFS and BFM

The highest BFS at 24 h was observed for M0S0 (182±22 MPa) (Fig. 4A). This was significantly higher than that of M6S10 (128±14 MPa, $p<0.001$), M6S5 (139±29 MPa, $p<0.001$), M3S10 (135±10 MPa, $p<0.001$), M3S5 (132±24 MPa, $p<0.001$), and PV (122±14 MPa, $p<0.001$). The experimental resin cements containing additives also exhibited a BFS comparable to that of PV. At 4 weeks, the highest BFS was observed for M0S0 (182±18.3 MPa).

The highest BFM at 24 h was observed for M0S0 (5.2±0.6 GPa) (Fig. 4B). The BFM of M6S10 (4.4±1.1 MPa) was comparable to that of PV (3.7±0.3 GPa, $p=0.204$) but lower than that of M3S10 (5.7±0.4 GPa, $p=0.005$) and M3S5 (5.4±0.3 GPa, $p=0.03$). At 4 weeks, the BFM of M0S0 (5.9±1.0 GPa) was significantly higher
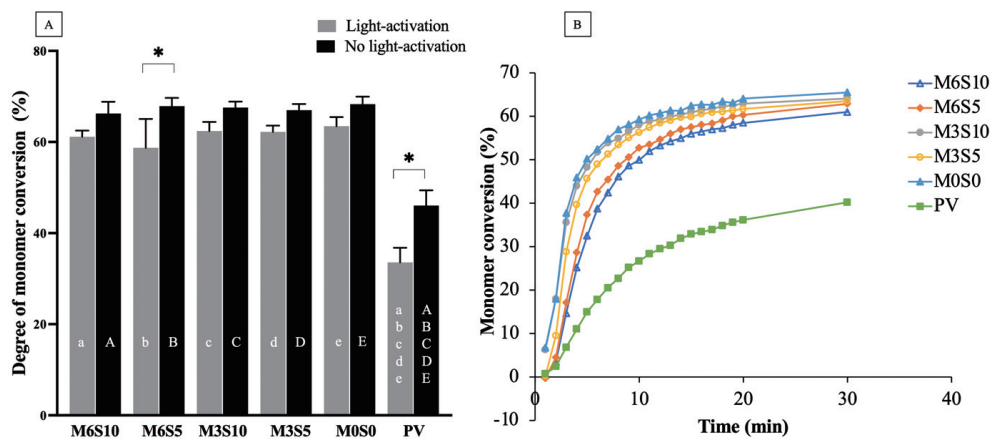

Fig. 3   (A) DC with and without light activation.
The same lowercase and uppercase letters indicate a significant difference ($p<0.05$) in DC with and without light activation, respectively. The asterisk (*) indicates $p<0.05$ for the DC with and without light activation of the same material. The error bars indicate SD ($n=5$). (B) DC of materials without light activation increasing over time.
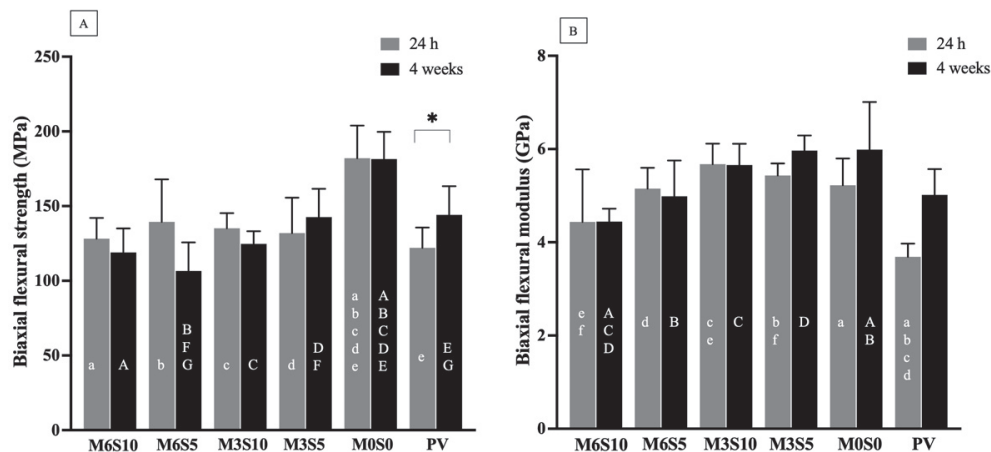

Fig. 4   (A) BFS and (B) BFM at 24 h and 4 weeks for all materials.
The same lowercase and uppercase letters indicate significant differences ($p<0.05$) among different materials at 24 h and 4 weeks, respectively. The asterisk (*) indicates $p<0.05$ when comparing values of the same material. The error bars indicate SDs ($n=7$).
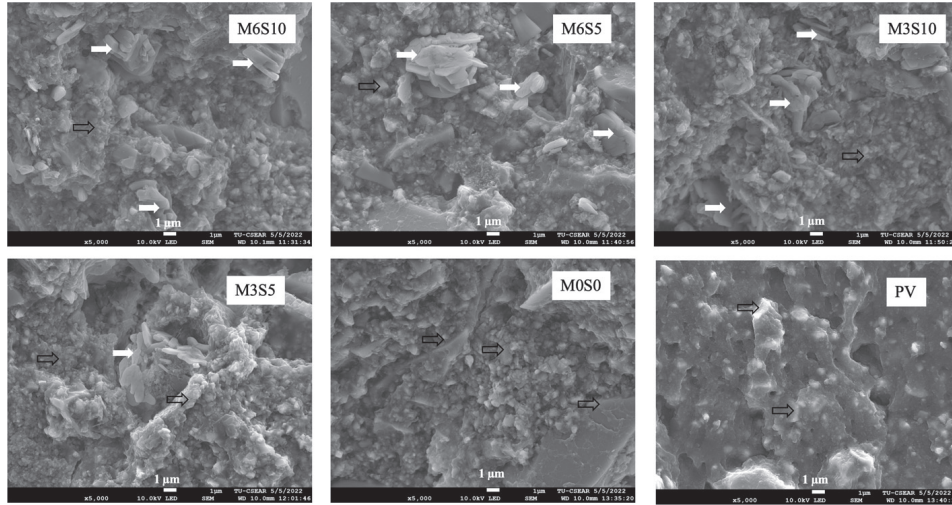
Fig. 5   Representative SEM images of fracture surfaces after BFS testing at 4 weeks for each material.
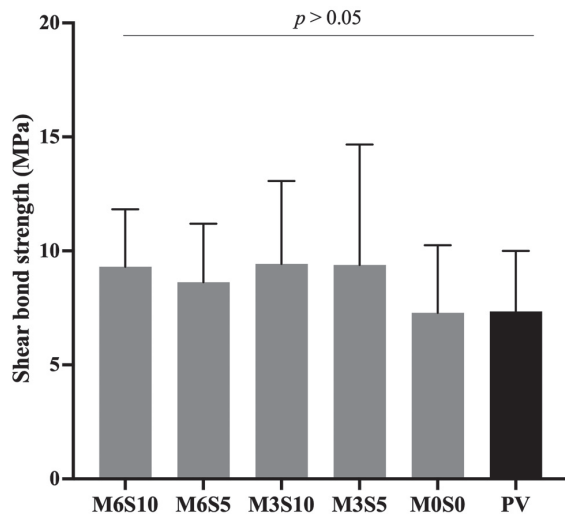The filled arrows indicate MCPM particles, while the unfilled arrows indicate the glass and resin matrix.

Fig. 6   SBS to ceramic at 24 h of all materials after immersion in water.
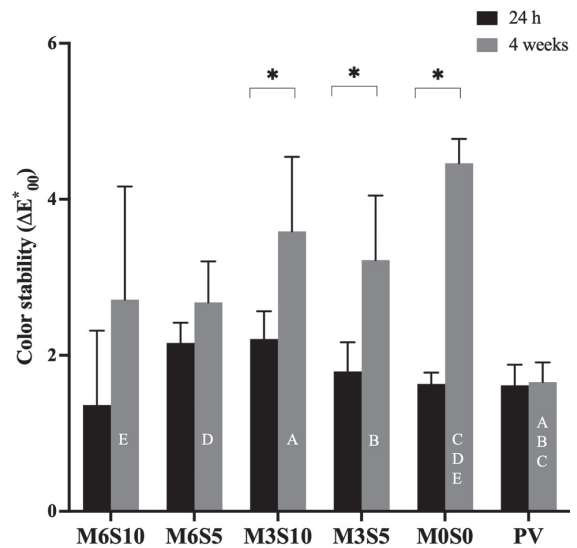The error bars indicate SD ($n=6$).

Fig. 7   Color difference (color stability) after immersion in water.
The same lowercase and uppercase letters indicate significant differences in color stability among the various materials at 24 h and 4 weeks, respectively. The asterisk (*) indicates $p<0.05$ when comparing two time points for a given material. The error bars indicate SD ($n=5$).

than that of M6S10 (4.4±0.3 GPa) and M6S5 (5.0±0.8 GPa). The fracture surface of the experimental resin cement contained the particles of MCPM, glass, and polymer matrix (Fig. 5). The fracture surface of PV was less irregular than the surface of the experimental resin cements.

Factorial analysis showed that an increase in the MCPM concentration from 3 to 6 wt% caused a significant reduction in the BFM by 15±11% and 19±6% at 24 h and 4 weeks, respectively. However, the effect of increasing the Sr-BGNP concentration from 5 to 10 wt% was negligible.

SBS to ceramic
The highest and lowest SBSs (Fig. 6) were observed for M3S10 (9.4±3.6 MPa) and PV (7.3±2.7 MPa). The SBS of PV was comparable to that of M6S10 (9.3±2.5 MPa, $p=0.915$), M6S5 (8.6±2.6 MPa, $p=0.986$), M3S10 (9.4±3.6 MPa, $p=0.894$), M3S5 (9.4±5.3 MPa, $p=0.902$), and M0S0 (7.3±3.0 MPa, $p>0.05$). No significant differences among

experimental materials were detected. The failure mode observed from the debonded interface was mostly mixed failure. Additionally, no significant effects of MCPM and Sr-BGNP concentrations on the SBS of experimental resin cements from the factorial analysis.

Color difference or color stability (ΔE_{00})

At 24 h, the color difference (ΔE_{00}) of all materials after immersion was comparable (Fig. 7). At 4 weeks, a significant increase in ΔE_{00} compared with that at 24 h was detected for M3S10 ($p=0.0159$), M3S5 ($p=0.0212$), and M0S0 ($p<0.0001$) but not the other materials. At 4 weeks, M0S0 exhibited the highest ΔE_{00} (4.5±0.3), which was significantly higher than that of PV (1.7±0.2, $p<0.001$), M6S10 (2.7±1.4, $p=0.030$) and M6S5 (2.7±0.5, $p=0.013$). Furthermore, the ΔE_{00} of PV was comparable to that of M6S10 ($p=0.2428$) and M6S5 ($p=0.9506$). No significant effect of the additives on the color change at 24 h was detected. At 4 weeks, the increase in MCPM

concentration slightly reduced the color change by 24±17%. The effect of the Sr-BGNP concentration was minimal.

Mass and volume changes

The early mass change of the set materials in water increased linearly with the square root of time, as expected with diffusion-controlled water sorption (Fig. 8A). The highest and lowest mass gains of the materials at 8 weeks were detected for M6S10 (1.63±0.11 wt%) and M0S0 (0.85±0.07 wt%), respectively. The mass gain of M6S10 was also significantly higher than that of M3S10 (1.22±0.13 wt%, $p=0.005$), M3S5 (1.10±0.23 wt%, $p=0.012$), M0S0 ($p<0.001$), and PV (1.16±0.08 wt%, $p=0.036$). The increase in the MCPM concentration enhanced the mass gain by approximately 35±20%, while the effect of increasing the Sr-BGNP concentration was negligible. The late-time volume gain of the materials was similar to the mass gain (Fig. 8B).
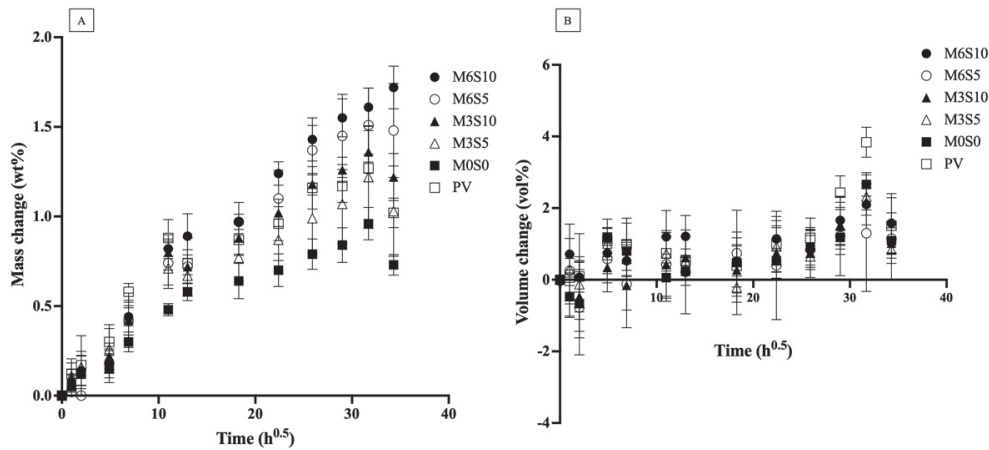

Fig. 8   (A) Mass and (B) volume changes of all materials versus the square root of immersion time in water, measured at up to 8 weeks.
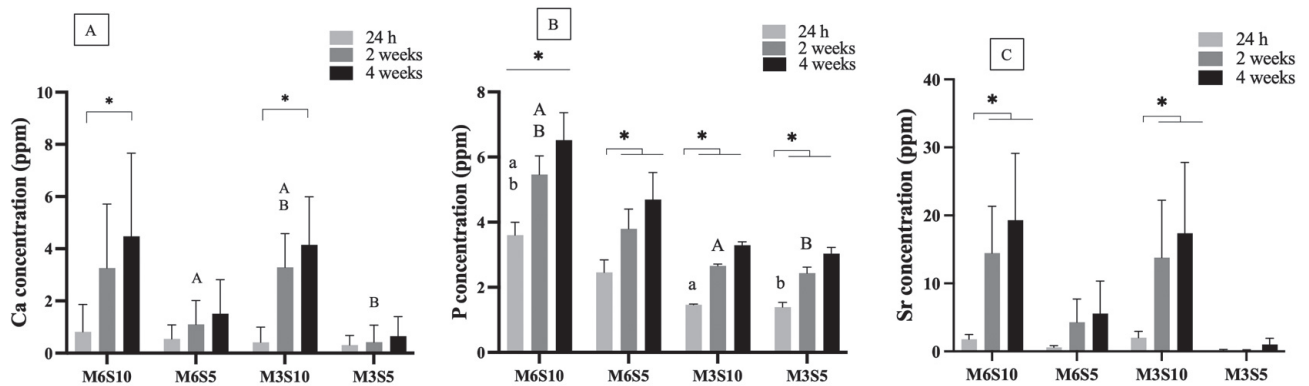The error bars indicate SD (n=5).

Fig. 9   Cumulative ion release of (A) Ca, (B) P, and (C) Sr ions at three different time points: 24 h, 2 weeks, and 4 weeks. The same lowercase and uppercase letters represent significant differences among different materials at 24 h and 2 weeks, respectively. However, no significant differences among the materials were detected at the 4-week time point. The asterisks (*) indicate $p<0.05$ when comparing the same material at different time points. The error bars indicate SD (n=5).
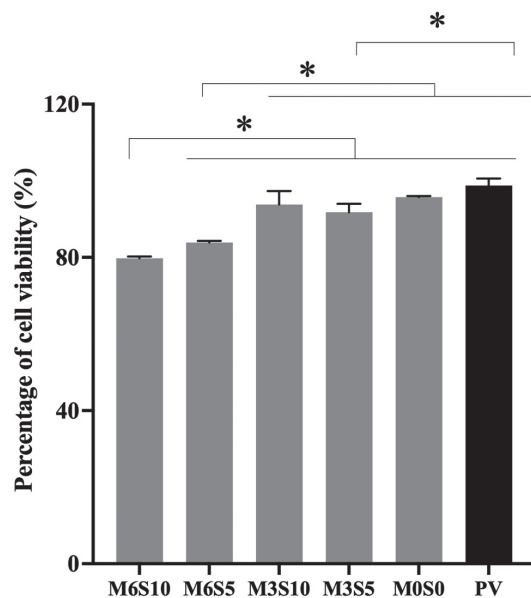
Fig. 10   The relative cell viability of fibroblasts exposed to material extracts. Asterisks (*) indicate $p<0.05$. The error bars indicate SD ($n=3$).

Ion release

Cumulative ion release from M0S0 and PV was not detected. The cumulative Ca ion release at 4 weeks (Fig. 9A) of M6S10 (8.2±2.5 ppm) was significantly higher than that of M6S5 (3.0±0.7 ppm, $p=0.047$) and M3S5 (1.5±0.2 ppm, $p=0.013$). M6S10 also exhibited the highest P release (6.5±0.9 ppm) and Sr release (19±9 ppm) at 4 weeks (Figs. 9B, C). Factorial analysis showed that doubling the Sr-BGNPs and MCPM concentrations enhanced the cumulative release of P ions by 74±13% and 24±18%, respectively. Additionally, increasing the concentration of Sr-BGNPs from 5 to 10 wt% substantially enhanced the cumulative release of Ca and Sr ions at 4 weeks by almost 4 times (223±53%) and 16 times (880±644%), respectively. The effect of increasing the MCPM concentration was negligible.

Cytotoxicity

The highest and lowest cell viability was observed in the presence of extracts for PV (98±1%) and M6S10 (78±1%), respectively (Fig. 10). The cell viability of M6S10 was significantly lower than that of M3S10 (94±4%, $p<0.001$), M3S5 (92±2%, $p<0.001$), M0S0 (96±1%, $p<0.001$), and PV ($p<0.001$). PV exhibited cell viability comparable to that of M3S10 ($p=0.0607$) and M0S0 ($p=0.797$). Doubling the MCPM concentration reduced the cell viability by 12±1%, but the effect of Sr-BGNPs was negligible.

DISCUSSION

This study formulated ion-releasing dual-cured resin cements. The effect of MCPM and Sr-BGNPs on physical properties and mechanical strength of the cements were also determined. The first null hypothesis was rejected

because the additives significantly affected properties such as the BFS and ion release of the experimental cements. Furthermore, the results indicated that the DC, BFS/BFM, SBS, mass/volume changes, ion release, and *in vitro* cytotoxicity of the experimental resin cements of all formulations were not similar to those of the commercial material. Hence, the second null hypothesis was also rejected.

It was proposed that a high monomer conversion could potentially lead to the enhanced mechanical strength with a low risk toxic monomer release for resin-based materials[44,45]. A study reported that adding strontium phosphates at 25 wt% into powder phase significantly decreased the DC of experimental resin composites upon light-curing, which could presumably due to the enhanced light scattering[15]. The additives employed in the current formulations showed negligible effects on the DC. This could be attributed to the use of additives at low concentrations. The DC of the experimental cements with or without light activation was higher than that of PV, which could be explained by the use of different base monomers. UDMA monomers often exhibit higher DCs than bisphenol A-glycidyl methacrylate (Bis-GMA) monomers due to the lower glass transition temperature of UDMA (–35°C) compared with to that of Bis-GMA (–8°C)[34,46]. Furthermore, the chain transfer reactions of the -NH- groups in UDMA could enhance the conversion of the monomers[46]. The use of UDMA as a base monomer was expected to enhance monomer conversion and reduce the concern regarding potential BPA impurities in Bis-GMA monomers[47].

Doubling the concentrations of Sr-BGNPs (from 5 to 10 wt%) and MCPM (from 3 to 6 wt%) in the current formulations showed no significant effect on the BFS. There was, however, a significant decrease in the BFS compared with that of the M0S0 formulation. The addition of MCPM and Sr-BGNPs reduced the BFS of the experimental cements by approximately 30 MPa. A primary cause for this reduction is likely the absence of silane-coupling agents on their surfaces. However, the additives were not silanized to enhance the release of ions upon exposure to water or oral fluid. Despite the negative effect of reactive fillers, the flexural strength of the materials was within the acceptable range (20 MPa) required by the ISO/TS 16506:2017[48]. This study's limitation was that the experimental resin cement pastes were prepared by hand-mixing, which may inevitably lead to air entrapment.

It was speculated that the increase in dark-cured polymerization could enhance polymer rigidity[49]. This may help mitigate the negative effects of hygroscopic expansion caused by hydrophilic fillers. Moreover, MCPM particles were still observed in the bulk of the materials even after 4 weeks. This observation suggests that the increased rigidity of the polymer network might also slow down water diffusion and limit filler dissolution. This could consequently facilitate the sustained release of ions without causing a rapid and substantial reduction in the strength of the materials. Long-term immersion for up to 6–12 months may be needed in future work to

determine the long-term strength of the materials.

The similarity in bonding performance between experimental cements and the commercial material could be attributed to the identical surface treatment protocol performed for all materials. Furthermore, the same adhesive monomer (10-MDP) was also contained in all groups. The obtained SBS was in accordance with that reported in other studies (2–15 MPa)[50,51]. The SBS was assessed at an early time point (24 h), following test type 1 in ISO/TS 11405:2015[52]. A longer aging period with thermocycling (*e.g.*, 10,000 to 30,000 cycles) may be needed to ensure the long-term bonding performance of the materials.

The addition of MCPM, a highly soluble calcium orthophosphate (Ca/P ratio=0.5), inevitably results in an increase in mass mainly due to water sorption. The degree of mass and volume changes in the experimental materials were found to be comparable to those of a resin composite reported in a previously published study (1 to 3 wt%)[53]. The absorbed water was expected to encourage hygroscopic expansion. This expansion may help relieve the polymerization shrinkage stress of resin-based materials[54]. The effect of Sr-BGNPs on the mass gain of the materials was minimal compared to the effect of MCPM. This could be potentially due to the low water solubility of Sr-BGNPs.

Marginal discoloration of indirect restorations caused by poor color stability of resin cement has been detected in 30% to 40% of restorations[55]. It was also proposed that the yellowish appearance of resin cements could be due to the degradation of residual amines and the oxidation of the remaining double bonds in the cements[55,56]. The color difference (ΔE_{00}) perceptibility and acceptability levels of tooth-colored materials are 0.8 and 1.8, respectively. At 24 h, all materials except for M6S5 and M3S10 exhibited values comparable with these values. At 4 weeks, the experimental resin cements showed a substantial increase in color difference, which was higher than the recommended maximum. A study showed that the color change of resin composites, containing bioactive glass (diameter of approximately 2 μm and 20–40 μm), increased from 2.6 to a range of 5.5–15.4 after immersion in water for 30 days[57]. The possible explanation for this could be the increase in surface irregularities caused by the dissolution of bioactive glass. Furthermore, the increase in color change was predominantly affected by the type of storage solution[58]. This is a variable that should be examined in future work. Additionally, the experimental resin cements may contain larger glass particles than commercial materials. It was suggested that the larger particle size in resin composites may reduce color stability upon water aging compared with composites containing smaller particle sizes[59,60]. The size and distribution of fillers in resin composites also affect the light reflectivity and optical properties of the materials[61].

Calcium and strontium release were substantially enhanced by increasing the concentration of Sr-BGNPs. It was hypothesized that the high surface area of nanoparticles, in combination with the surface-doped

Ca and Sr, could enable a high release of ions upon exposure to fluid[62]. The ability to promote ion release from materials is expected to enable remineralizing/antibacterial actions and acid neutralization[12], which should be examined in a long-term study. The release of nanoparticles, ions, or residual monomers from the experimental resin cements may induce cytotoxic effects on gingival tissues. The level of reactive fillers in the current study exhibited low *in vitro* toxic effects on cells. The diffusion of ions and Sr-BGNPs may be limited by the polymerized network of resin cements. A study showed that the release of Sr^{2+} into culture media at a concentration of 2 to 6 μg/mL resulted in low cytotoxic effects[29]. Significant toxic effects have been induced by the bioactive glass with particle diameters that were smaller than 10 nm or larger than 10 μm[63]. Hence, the use of bioactive glass with a diameter of approximately 100 to 200 nm in the current study may result in cytotoxic effects that are below an unacceptable level. Increasing the concentration of hydrophilic MCPM may result in cytotoxic effects due to the increase in water plasticization or the degradation of the polymer network. This may increase the risk of releasing toxic monomers[64]. The composition of the extracts should be confirmed using HPLC in future studies.

It should be mentioned that the current study is an *in vitro* study, thus, further *in vivo* tests are required to determine the clinical benefits. It was, however, anticipated that the use of ion-releasing resin cement could potentially help decrease the risk of secondary caries, which is one of the common reasons for the failure of fixed protheses treatments.

CONCLUSION

This study successfully prepared ion-releasing resin cements containing Sr-BGNPs and MCPM. The experimental cements exhibited a higher DC compared to the commercial product. The experimental materials also demonstrated lower color stability compared to the commercial material, but they showed ion release action and a low cytotoxic effect. Furthermore, the additives showed no detrimental effects on monomer conversion. The additive, however, reduced the strength of the experimental materials, but strength values still remained within the acceptable range.

conducting the cytotoxicity test.

REFERENCES

1) Politano G, Fabianelli A, Papacchini F, Cerutti A. The use of bonded partial ceramic restorations to recover heavily compromised teeth. Int J Esthet Dent 2016; 11: 314-336.
2) Wong FMF, Ng YTY, Leung WK. Oral health and its associated factors among older institutionalized residents —A systematic review. Int J Environ Res Public Health 2019; 16: 4132.
3) Marchini L, Ettinger R, Hartshorn J. Personalized dental caries management for frail older adults and persons with special needs. Dent Clin North Am 2019; 63: 631-651.
4) D'Arcangelo C, Zarow M, De Angelis F, Vadini M, Paolantonio M, Giannoni M, *et al.* Five-year retrospective clinical study of indirect composite restorations luted with a light-cured composite in posterior teeth. Clin Oral Investig 2014; 18: 615-624.
5) Alenezi A, Alkhudhayri O, Altowaijri F, Aloufi L, Alharbi F, Alrasheed M, *et al.* Secondary caries in fixed dental prostheses: Long-term clinical evaluation. Clin Exp Dent Res 2023; 9: 249-257.
6) Wu C, Kim MJ, Mangal U, Seo JY, Kim JY, Kim J, *et al.* Effect of bacterial resistant zwitterionic derivative incorporation on the physical properties of resin-modified glass ionomer luting cement. Sci Rep 2023; 13: 3589.
7) Anami LC, Pereira CA, Guerra E, Assuncao e Souza RO, Jorge AO, Bottino MA. Morphology and bacterial colonisation of tooth/ceramic restoration interface after different cement excess removal techniques. J Dent 2012; 40: 742-749.
8) Pereira S, Anami LC, Pereira CA, Souza R, Kantorski KZ, Bottino MA, *et al.* Bacterial colonization in the marginal region of ceramic restorations: Effects of different cement removal methods and polishing. Oper Dent 2016; 41: 642-654.
9) Alomari Q, Al-Saiegh F, Qudeimat M, Omar R. Recurrent caries at crown margins: Making a decision on treatment. Med Princ Pract 2009; 18: 187-192.
10) AlSahafi R, Mitwalli H, Alhussein A, Melo MAS, Martinho F, Lynch CD, *et al.* Novel rechargeable nanostructured calcium phosphate crown cement with long-term ion release and antibacterial activity to suppress saliva microcosm biofilms. J Dent 2022; 122: 104140.
11) Pellizzari VA, Michels AC, Luiz ST, de Souza EM, Tabchoury C, Rached RN. Fluoride ion release of self-adhesive resin cements and their potential to inhibit in situ enamel and dentin demineralization. Oper Dent 2017; 42: 548-558.
12) Braga RR. Calcium phosphates as ion-releasing fillers in restorative resin-based materials. Dent Mater 2019; 35: 3-14.
13) Pitts NB, Zero DT, Marsh PD, Ekstrand K, Weintraub JA, Ramos-Gomez F, *et al.* Dental caries. Nat Rev Dis Primers 2017; 3: 17030.
14) Aljabo A, Abou Neel EA, Knowles JC, Young AM. Development of dental composites with reactive fillers that promote precipitation of antibacterial-hydroxyapatite layers. Mater Sci Eng C Mater Biol Appl 2016; 60: 285-292.
15) Panpisut P, Liaqat S, Zacharaki E, Xia W, Petridis H, Young AM. Dental composites with calcium/strontium phosphates and polylysine. PLoS One 2016; 11: e0164653.
16) Panpisut P, Suppapatpong T, Rattanapan A, Wongwarawut P. Monomer conversion, biaxial flexural strength, apatite forming ability of experimental dual-cured and self-adhesive dental composites containing calcium phosphate and nisin. Dent Mater J 2021; 40: 399-406.
17) Chanachai S, Chaichana W, Insee K, Benjakul S, Aupaphong V, Panpisut P. Physical/mechanical and antibacterial properties of orthodontic adhesives containing calcium

phosphate and nisin. J Funct Biomater 2021; 12: 73.
18) Chaichana W, Insee K, Chanachai S, Benjakul S, Aupaphong V, Naruphontjirakul P, *et al.* Physical/mechanical and antibacterial properties of orthodontic adhesives containing sr-bioactive glass nanoparticles, calcium phosphate, and andrographolide. Sci Rep 2022; 12: 6635.
19) Ferracane JL. Hygroscopic and hydrolytic effects in dental polymer networks. Dent Mater 2006; 22: 211-222.
20) Mirchandani B, Padunglappisit C, Toneluck A, Naruphontjirakul P, Panpisut P. Effects of sr/f-bioactive glass nanoparticles and calcium phosphate on monomer conversion, biaxial flexural strength, surface microhardness, mass/volume changes, and color stability of dual-cured dental composites for core build-up materials. Nanomaterials (Basel) 2022; 12: 1897.
21) Kantrong N, Khongkhaphet K, Sitornsud N, Lo-Apirukkul P, Phanprom W, Rojviriya C, *et al.* Synchrotron radiation analysis of root dentin: The roles of fluoride and calcium ions in hydroxyapatite remineralization. J Synchrotron Radiat 2022; 29: 496-504.
22) Lamont RJ, Koo H, Hajishengallis G. The oral microbiota: Dynamic communities and host interactions. Nat Rev Microbiol 2018; 16: 745-759.
23) Simila HO, Boccaccini AR. Sol-gel bioactive glass containing biomaterials for restorative dentistry: A review. Dent Mater 2022; 38: 725-747.
24) Brauer DS, Karpukhina N, Kedia G, Bhat A, Law RV, Radecka I, *et al.* Bactericidal strontium-releasing injectable bone cements based on bioactive glasses. J R Soc Interface 2013; 10: 20120647.
25) Baheiraei N, Eyni H, Bakhshi B, Najafloo R, Rabiee N. Effects of strontium ions with potential antibacterial activity on in vivo bone regeneration. Sci Rep 2021; 11: 8745.
26) Manoochehri H, Ghorbani M, Moosazadeh Moghaddam M, Nourani MR, Makvandi P, Sharifi E. Strontium doped bioglass incorporated hydrogel-based scaffold for amplified bone tissue regeneration. Sci Rep 2022; 12: 10160.
27) Jayasree R, Kumar TSS, Mahalaxmi S, Abburi S, Rubaiya Y, Doble M. Dentin remineralizing ability and enhanced antibacterial activity of strontium and hydroxyl ion co-releasing radiopaque hydroxyapatite cement. J Mater Sci Mater Med 2017; 28: 95.
28) Egbuna C, Parmar VK, Jeevanandam J, Ezzat SM, Patrick-Iwuanyanwu KC, Adetunji CO, *et al.* Toxicity of nanoparticles in biomedical application: Nanotoxicology. J Toxicol 2021; 2021: 9954443.
29) Naruphontjirakul P, Porter AE, Jones JR. In vitro osteogenesis by intracellular uptake of strontium containing bioactive glass nanoparticles. Acta Biomater 2018; 66: 67-80.
30) Panpisut P, Khan MA, Main K, Arshad M, Xia W, Petridis H, *et al.* Polymerization kinetics stability, volumetric changes, apatite precipitation, strontium release and fatigue of novel bone composites for vertebroplasty. PLoS One 2019; 14: e0207965.
31) Delgado AHS, Young AM. Methacrylate peak determination and selection recommendations using atr-ftir to investigate polymerisation of dental methacrylate mixtures. PLoS One 2021; 16: e0252999.
32) British Standard. Bs en iso 4049:2019. Dentistry—Polymer-based restorative materials. Switzerland: BSI Standards; 2019.
33) Aldhafyan M, Silikas N, Watts DC. Influence of curing modes on thermal stability, hardness development and network integrity of dual-cure resin cements. Dent Mater 2021; 37: 1854-1864.
34) Walters NJ, Xia W, Salih V, Ashley PF, Young AM. Poly(propylene glycol) and urethane dimethacrylates improve conversion of dental composites and reveal complexity of cytocompatibility testing. Dent Mater 2016; 32: 264-277.

35) Kim DS, Ahn JJ, Bae EB, Kim GC, Jeong CM, Huh JB, *et al.* Influence of non-thermal atmospheric pressure plasma treatment on shear bond strength between y-tzp and self-adhesive resin cement. Materials (Basel) 2019; 12: 3321.

36) Ardu S, Duc O, Di Bella E, Krejci I. Color stability of recent composite resins. Odontology 2017; 105: 29-35.

37) Panpisut P, Toneluck A. Monomer conversion, dimensional stability, biaxial flexural strength, and fluoride release of resin-based restorative material containing alkaline fillers. Dent Mater J 2020; 39: 608-615.

38) Potiprapanpong W, Thepveera W, Khamsuk C, Channasanon S, Tanodekaew S, Patntirapong S, *et al.* Monomer conversion, dimensional stability, biaxial flexural strength, ion release, and cytotoxicity of resin-modified glass ionomer cements containing methacrylate-functionalized polyacids and spherical pre-reacted glass fillers. Polymers (Basel) 2021; 13: 2742.

39) British Standard. 10993–5: 2009 biological evaluation of medical devices. Part 5: tests for in vitro cytotoxicity. London, UK: BSI Standards Limited; 2009.

40) Pagano S, Lombardo G, Balloni S, Bodo M, Cianetti S, Barbati A, *et al.* Cytotoxicity of universal dental adhesive systems: Assessment in vitro assays on human gingival fibroblasts. Toxicol In Vitro 2019; 60: 252-260.

41) Faul F, Erdfelder E, Lang AG, Buchner A. G*power 3: A flexible statistical power analysis program for the social, behavioral, and biomedical sciences. Behav Res Methods 2007; 39: 175-191.

42) Kim HY. Statistical notes for clinical researchers: Sample size calculation 3. Comparison of several means using one-way anova. Restor Dent Endod 2016; 41: 231-234.

43) Thanasrisuebwong P, Jones JR, Eiamboonsert S, Ruangsawasdi N, Jirajariyavej B, Naruphontjirakul P. Zinc-containing sol-gel glass nanoparticles to deliver therapeutic ions. Nanomaterials (Basel) 2022; 12: 1691.

44) Kitagawa FA, Leite ML, Soares IPM, Anselmi C, de Oliveira Ribeiro RA, Hebling J, *et al.* Influence of ceramic veneer on the transdentinal cytotoxicity, degree of conversion and bond strength of light-cured resin cements to dentin. Dent Mater 2022; 38: e160-e173.

45) Martinez-Gonzalez M, Fidalgo-Pereira RC, Torres O, Silva F, Henriques B, Ozcan M, *et al.* Toxicity of resin-matrix cements in contact with fibroblast or mesenchymal cells. Odontology 2023; 111: 310-327.

46) Par M, Spanovic N, Taubök TT, Attin T, Tarle Z. Degree of conversion of experimental resin composites containing bioactive glass 45s5: The effect of post-cure heating. Sci Rep 2019; 9: 17245.

47) Lofroth M, Ghasemimehr M, Falk A, Vult von Steyern P. Bisphenol a in dental materials —Existence, leakage and biological effects. Heliyon 2019; 5: e01711.

48) British Standard. Pd iso/ts 16506: 2017. Dentistry—Polymer-based luting materials containing adhesive components. Switzerland: BSI Standards Limited; 2017.

49) Rizzante FAP, Locatelli PM, Porto TS, Borges AFS, Mondelli RFL, Ishikiriama SK. Physico-mechanical properties of resin cement light cured through different ceramic spacers. J Mech Behav Biomed Mater 2018; 85: 170-174.

50) Charasseangpaisarn T, Krassanairawiwong P, Sangkanchanavanich C, Kurjirattikan A, Kunyawatyuwapong K, Tantivasin N. The influence of different surface cleansing agents on shear bond strength of contaminated lithium disilicate ceramic: An in vitro study. Int J Dent 2021; 2021: 7112400.

51) Li R, Ma SQ, Zang CC, Zhang WY, Liu ZH, Sun YC, *et al.* Enhanced bonding strength between lithium disilicate ceramics and resin cement by multiple surface treatments after thermal cycling. PLoS One 2019; 14: e0220466.

52) British Standard. Pd iso/ts 11405:2015. Dentistry—Testing of adhesion to tooth structure. Switzerland: BSI Standards; 2015.

53) Alshali RZ, Salim NA, Satterthwaite JD, Silikas N. Long-term sorption and solubility of bulk-fill and conventional resin-composites in water and artificial saliva. J Dent 2015; 43: 1511-1518.

54) Bociong K, Szczesio A, Sokolowski K, Domarecka M, Sokolowski J, Krasowski M, *et al.* The influence of water sorption of dental light-cured composites on shrinkage stress. Materials (Basel) 2017; 10: 1142.

55) Ramos NC, Luz JN, Valera MC, Melo RM, Saavedra G, Bresciani E. Color stability of resin cements exposed to aging. Oper Dent 2019; 44: 609-614.

56) Saati K, Valizadeh S, Anaraki SN, Moosavi N. Effect of aging on color stability of amine-free resin cement through the ceramic laminate veneer. Dent Res J (Isfahan) 2021; 18: 99.

57) Tuncdemir MT, Gulbahce N. Addition of antibacterial agent effect on color stability of composites after immersion of different beverages. J Esthet Restor Dent 2019; 31: 508-513.

58) Tavangar M, Bagheri R, Kwon TY, Mese A, Manton DJ. Influence of beverages and surface roughness on the color change of resin composites. J Investig Clin Dent 2018; 9: e12333.

59) Malekipour MR, Sharafi A, Kazemi S, Khazaei S, Shirani F. Comparison of color stability of a composite resin in different color media. Dent Res J (Isfahan) 2012; 9: 441-446.

60) Elfakhri F, Alkahtani R, Li C, Khaliq J. Influence of filler characteristics on the performance of dental composites: A comprehensive review. Ceram Int 2022; 48: 27280-27294.

61) Lim YK, Lee YK, Lim BS, Rhee SH, Yang HC. Influence of filler distribution on the color parameters of experimental resin composites. Dent Mater 2008; 24: 67-73.

62) Ji L, Xu T, Gu J, Liu Q, Zhou S, Shi G, *et al.* Preparation of bioactive glass nanoparticles with highly and evenly doped calcium ions by reactive flash nanoprecipitation. J Mater Sci Mater Med 2021; 32: 48.

63) Naruphontjirakul P, Li S, Pinna A, Barrak F, Chen S, Redpath AN, *et al.* Interaction of monodispersed strontium containing bioactive glass nanoparticles with macrophages. Biomater Adv 2022; 133: 112610.

64) Agha A, Parker S, Parkinson EK, Patel M. Characteristics of experimental resin-modified glass-ionomer cements, containing alternate monomers to hema. Dent Mater 2021; 37: 1542-1552.